Journal of Computational and Applied Mathematics 401 (2022) 113766

Contents lists available at ScienceDirect

Journal of Computational and Applied Mathematics

journal homepage: www.elsevier.com/locate/cam

High order accurate in time, fourth order finite difference schemes for the harmonic mapping flow

Zeyu Xia [a], Cheng Wang [b,*], Liwei Xu [c], Zhengru Zhang [d]

[a] School of Mathematical Sciences, University of Electronic Science and Technology of China, Chengdu, 610054, China
[b] Mathematics Department, University of Massachusetts, North Dartmouth, MA 02747, USA
[c] School of Mathematical Sciences, University of Electronic Science and Technology of China, Chengdu, China 610054, China
[d] School of Mathematical Sciences, Beijing Normal University, Beijing 100875, China

ARTICLE INFO

Article history:
Received 1 March 2020

MSC:
35K35
35K55
65M06
65M12

Keywords:
Harmonic mapping flow
Third order multi-step scheme
Fourth order long stencil difference approximation
Optimal rate convergence analysis

ABSTRACT

In this paper, a fully discrete numerical scheme is proposed and analyzed for the harmonic mapping flow, with the fourth order spatial accuracy and higher than third order temporal accuracy. The fourth order spatial accuracy is realized via a long stencil finite difference, and the boundary extrapolation is implemented by making use of higher order Taylor expansion. Meanwhile, the high order (third or fourth order) temporal accuracy is based on a semi-implicit algorithm, which uses a combination of explicit Adams–Bashforth extrapolation for the nonlinear terms and implicit Adams–Moulton interpolation for the viscous diffusion term, with the corresponding integration formula coefficients. Both the consistency, linearized stability analysis and optimal rate convergence estimate (in the $\ell^\infty(0,T;\ell^2)\cap\ell^2(0,T;H_h^1)$ norm) are provided. A few numerical examples are also presented in this article.

1. Introduction

The liquid crystal is a very important model with potential applications in physics and chemistry [1,2]. The prototypic for continuum models in ferromagnetics [3] and liquid crystal theory [4,5] is based on the following energy, known as harmonic maps into spheres [6]:

$$E(\mathbf{u})=\frac{1}{2}\int_\Omega |\nabla\mathbf{u}|^2 d\mathbf{x}. \tag{1.1}$$

In turn, its long-time behavior into spheres [6] is given by

$$\begin{aligned} &\mathbf{u}_t-\Delta\mathbf{u}=|\nabla\mathbf{u}|^2\mathbf{u}, \quad \text{in } \Omega\times[0,T),\\ &\partial_n\mathbf{u}=0, \quad \text{on } \partial\Omega\times[0,T),\\ &\mathbf{u}(0,\cdot)=\mathbf{u}_0, \quad \text{in } \Omega. \end{aligned} \tag{1.2}$$

Here, $\Omega\subset\mathbb{R}^d(d=1,2,3)$ is the domain, $\partial\Omega$ represents the boundary, and $\mathbf{n}$ is the outer unit norm vector of $\partial\Omega$.

The solution for (1.2) has been extensively analyzed in many exiting works. An obvious conclusion which can be verified by fundamental PDE analysis is that, if $|\mathbf{u}|=1$ at the initial time, and then $|\mathbf{u}|=1$ at any later time. This property could

* Corresponding author.
E-mail addresses: zeyuxia@std.uestc.edu.cn (Z. Xia), cwang1@umassd.edu (C. Wang), xul@uestc.edu.cn (L. Xu), zrzhang@bnu.edu.cn (Z. Zhang).

https://doi.org/10.1016/j.cam.2021.113766
0377-0427/

be verified by taking inner product with $\mathbf{u}$ on both sides. The global existence of weak solution for a linearized eigenvalue PDE $\mathbf{u}_t - \Delta\mathbf{u} - \lambda\mathbf{u} = 0$ has been proved in [7], under the requirement that $|\mathbf{u}| = 1$ and λ satisfies certain conditions formulated in the reference. Furthermore, the partial regularity results of this equation have been established in [8]. More related works about (1.2) can be found in [9–12].

In fact, the energy dissipation property of the harmonic mapping flow (1.2) could be observed in the following fact. Under the point-wise constraint $|\mathbf{u}| = 1$, we see that the dynamic equation in (1.2) could be equivalently rewritten as

$$\mathbf{u}_t = -\mathbf{u} \times (\mathbf{u} \times \Delta\mathbf{u}). \tag{1.3}$$

In turn, taking inner product with (1.3) by $-\Delta\mathbf{u}$, we arrive at the following energy dissipation law:

$$\frac{1}{2}\frac{d}{dt}E(\mathbf{u}(t)) = \Big(\mathbf{u} \times (\mathbf{u} \times \Delta\mathbf{u}),\, \Delta\mathbf{u}\Big) \le 0. \tag{1.4}$$

Also see the related works [13,14] for the Landau–Lifshitz system in the micromagnetics model.

Since an explicit form of the exact solution for (1.2) is not available, an efficient numerical scheme is highly desirable. Among the existing numerical works, the high-order-accurate schemes are very limited. Bartels presented a stable and convergent finite element approximation scheme in [15]. Alouges used finite difference methods, which are convergent in a continuous setting [4]. Vese and Osher also solved a similar equation, so-called p-harmonic flows, whose energy function is expressed as $E_p(\mathbf{u}) = \int_\Omega |\nabla\mathbf{u}|^p d\mathbf{x}$, by finite difference algorithm in [16]. Also see [17,18] for the finite element approximations to the p-harmonic flow. A more recent work [19] reports the motion of singularity development for the harmonic mapping, based on a first order semi-implicit temporal discretization and the standard centered difference spatial approximation. Of course, many other numerical methods can also be used to solve this equation, such as the Fourier pseudo-spectral approximation and others.

In fact, a fourth order and even more accurate spatial discretization is highly desirable, for the sake of its ability to capture the more detailed structure with a reduced computational cost. In this paper, we propose and analyze high order (third or fourth order) accurate in time, fourth order long stencil finite difference methods for the harmonic mapping flow (1.2), with the stability and convergence established at a theoretical level. As is well known, the finite difference approximation has its advantage of being straightforward in the consistency analysis, based on a direct application of Taylor expansion. There have been quite a few existing works of fourth order long stencil difference schemes applied to various nonlinear PDEs, such as incompressible fluid equations [20–23], Cahn–Hilliard equation [24], and Maxwell equation [25]. We observe that, an application of such a long stencil difference approximation to the harmonic mapping flow is appropriate, due to the homogeneous Neumann boundary condition. In the temporal discretization, we adopt an explicit multi-step Adams–Bashforth approach for the nonlinear gradient terms and an implicit Adams–Moulton method for the diffusion term. This approach has the advantage of handling the nonlinear terms in an inexpensive way, while providing the stability associated with implicit methods. On the other hand, a straightforward application of high order accurate Adams–Bashforth/Adams–Moulton will lead to an unstable method, as demonstrated in an existing work [26]. Instead, we look for an Adams–Moulton interpolation so that the diffusion term is more focused on the time step t^{n+1}, i.e., the coefficient at time step t^{n+1} dominates the sum of the rest of diffusion coefficients. It is discovered that the Adams–Moulton interpolation which involves the time node points t^{n+1}, t^{n-1} and t^{n-3} gives the corresponding coefficients as 2/3, 5/12, −1/12, respectively, which satisfies the unconditional stability condition, in the third order temporally accurate algorithm. Stability and convergence for such a multi-step, semi-implicit method have been provided for the viscous Burgers' equation [26] and incompressible Navier–Stokes equation [27]. Its application to the harmonic mapping flow (1.2) will be analyzed in this work, with an optimal rate convergence estimate available. The fourth order accurate algorithm could also be derived in a similar fashion.

This article is organized as follows. The numerical scheme is proposed in Section 2, with the main theoretical results stated. The detailed convergence analysis and error estimate is provided in Section 3. Some numerical results are presented in Section 4. Finally, some concluding remarks are made in Section 5.

2. The numerical scheme and the main theoretical result

The long stencil fourth order finite difference formula is derived by the Taylor expansion for any test function. Over a one-dimensional domain $\Omega = (0, 1)$, we use the cell-centered grid points $x_{i+1/2} = (i + 1/2)h$, with $h = \frac{1}{N}$, with N the number of numerical mesh cells. The fourth order approximations to the first and second order derivatives, over a uniform cell-centered grid, are given by

$$\begin{aligned}\mathcal{D}^1_{x,(4)} f_{i+1/2} &= \tilde{D}_x(1 - \frac{h^2}{6}D_x^2)f_{i+1/2} = \frac{f_{i-3/2} - 8f_{i-1/2} + 8f_{i+3/2} - f_{i+5/2}}{12h} \\ &= f'(x_{i+1/2}) + O(h^4),\end{aligned} \tag{2.1}$$

$$\begin{aligned}\mathcal{D}^2_{x,(4)} f_{i+1/2} &= D_x^2(1 - \frac{h^2}{12}D_x^2)f_{i+1/2} = \frac{-f_{i-3/2} + 16f_{i-1/2} - 30f_{i+1/2} + 16f_{i+3/2} - f_{i+5/2}}{12h^2} \\ &= f''(x_{i+1/2}) + O(h^4),\end{aligned} \tag{2.2}$$

where $\tilde{D}_x$ and D_x^2 are the standard centered difference approximation to the first and second order derivatives, respectively. See the detailed derivations in the related Refs. [28–31]. These long stencil fourth order finite difference approximations have been extensively applied to different types of partial differential equations (PDEs), such as incompressible Boussinesq equation [21,23], three-dimensional geophysical fluid models [20,22], and the Maxwell equation [25].

An extension to the three dimensional domain $\Omega = (0, 1)^3$, with the cell-centered grid points $(x_{i+1/2}, y_{j+1/2}, z_{k+1/2})$, is straightforward. The corresponding difference operators in the y and z directions, namely $\mathcal{D}_{y,(4)}$, $\mathcal{D}^2_{y,(4)}$, $\mathcal{D}_{z,(4)}$, $\mathcal{D}^2_{z,(4)}$, could be similarly defined. In turn, we denote $\Delta_{h,(4)} = \mathcal{D}^2_{x,(4)} + \mathcal{D}^2_{y,(4)} + \mathcal{D}^2_{z,(4)}$. A careful calculation reveals that $\mathcal{D}^2_{x,(4)} f = (D_x^2 - \frac{h^2}{12} D_x^4) f$, in which D_x^2 is the standard centered difference operator. Furthermore, both operators correspond to non-positive eigenvalues associated with the Fourier Cosine eigenvectors, and this subtle fact will play an important role in the stability and convergence analysis. Also see the related works for the Fourier pseudo-spectral numerical methods [32–40].

At each cell-centered grid point $(x_{i+1/2}, y_{j+1/2}, z_{k+1/2})$, the nonlinear terms are evaluated as follows.

$$\begin{aligned}
(|\nabla_{h,(4)}\mathbf{u}|^2\mathbf{u})_{i+1/2,j+1/2,k+1/2} &= (|\nabla_{h,(4)}\mathbf{u}|^2)_{i+1/2,j+1/2,k+1/2}\mathbf{u}_{i+1/2,j+1/2,k+1/2}, \\
|\nabla_{h,(4)}\mathbf{u}|^2 &= |\nabla_{h,(4)}u|^2 + |\nabla_{h,(4)}v|^2 + |\nabla_{h,(4)}w|^2, \\
(|\nabla_{h,(4)}f|^2)_{i+1/2,j+1/2,k+1/2} &= (\mathcal{D}^1_{x,(4)}f)^2_{i+1/2,j+1/2,k+1/2} + (\mathcal{D}^1_{y,(4)}f)^2_{i+1/2,j+1/2,k+1/2} \\
&\quad + (\mathcal{D}^1_{z,(4)}f)^2_{i+1/2,j+1/2,k+1/2}.
\end{aligned} \tag{2.3}$$

The following fully discrete numerical scheme is proposed, with third order temporal accuracy and fourth order long stencil difference spatial approximation:

$$\begin{aligned}
&\frac{\mathbf{u}^{n+1} - \mathbf{u}^n}{\Delta t} - \Delta_{h,(4)}\Big(\frac{2}{3}\mathbf{u}^{n+1} + \frac{5}{12}\mathbf{u}^{n-1} - \frac{1}{12}\mathbf{u}^{n-3}\Big) \\
&= \frac{23}{12}|\nabla_{h,(4)}\mathbf{u}^n|^2\mathbf{u}^n - \frac{4}{3}|\nabla_{h,(4)}\mathbf{u}^{n-1}|^2\mathbf{u}^{n-1} + \frac{5}{12}|\nabla_{h,(4)}\mathbf{u}^{n-2}|^2\mathbf{u}^{n-2}.
\end{aligned} \tag{2.4}$$

Moreover, determination of $\mathbf{u}$ at "ghost" points is needed at each boundary section to implement (2.4). In general, using fewer interior points may lead to improved stability for a given order approximation. For brevity of the presentation we concentrate on the boundary section Γ_z where $z = 0$.

Because of the Neumann boundary condition given by (1.2), the value of $\mathbf{u}$ on the boundary is not known explicitly, only its normal derivative. In turn, (2.4) is applied at every interior computational point $(x_{i+1/2}, y_{j+1/2}, z_{k+1/2})$, $0 \le i, j, k \le N-1$. This fact requires one to determine two "ghost" point values, $\mathbf{u}_{i+1/2,j+1/2,-1/2}$ and $\mathbf{u}_{i+1/2,j+1/2,-3/2}$, to carry out (2.4). We begin with one-sided approximations around the boundary section Γ_z. For simplicity of presentation, we only focus on the variable u; the corresponding derivation could be extended to v and w in a straightforward way, since all these variables are evaluated at the same cell-centered mesh points. Local Taylor expansion near the boundary gives

$$u_{i+1/2,j+1/2,-1/2} = u_{i+1/2,j+1/2,1/2} - h\partial_z u_{i+1/2,j+1/2,0} - \frac{h^3}{24}\partial_z^3 u_{i+1/2,j+1/2,0} + O(h^5), \tag{2.5}$$

$$u_{i+1/2,j+1/2,-3/2} = u_{i+1/2,j+1/2,3/2} - 3h\partial_z u_{i+1/2,j+1/2,0} - \frac{9h^3}{8}\partial_z^3 u_{i+1/2,j+1/2,0} + O(h^5). \tag{2.6}$$

The term $\partial_z u_{i+1/2,j+1/2,0}$ in (2.5) and (2.6) is known from the homogeneous Neumann boundary condition (1.2). It remains to determine $\partial_z^3 \partial_z u_{i+1/2,j+1/2,0}$, for which we use information from the PDE and its derivatives. Applying ∂_z to the first evolutionary equation in (1.2) along Γ_z gives

$$u_{zt} - |\nabla\mathbf{u}|^2 u_z - 2u(\nabla u \cdot \nabla u_z + \nabla v \cdot \nabla v_z + \nabla w \cdot \nabla w_z) = u_{zxx} + u_{zyy} + \partial_z^3 u, \quad \text{on } \Gamma_z. \tag{2.7}$$

The first two terms on the left-hand side as well as the first two terms on the right-hand side of (2.7) disappear, due to the homogeneous Neumann boundary condition for u. For the third term on the left hand side, we observe that

$$\nabla u \cdot \nabla u_z = u_x \cdot u_{zx} + v_x \cdot v_{zx} + w_x \cdot w_{zx} = 0, \quad \text{on } \Gamma_z, \tag{2.8}$$

since $u_z = v_z = w_z = 0$ on the boundary section. Similar derivations could be made to the two other terms on the left hand side:

$$\nabla v \cdot \nabla v_z = 0, \quad \nabla w \cdot \nabla w_z = 0, \quad \text{on } \Gamma_z. \tag{2.9}$$

Combining all these arguments and substituting them back into (2.7), $\partial_z^3 u$ is approximated along Γ_z by

$$\partial_z^3 u_{i+1/2,j+1/2,0} = 0. \tag{2.10}$$

Subsequently, plugging (2.10) back into (2.5) and (2.6), we have

$$u_{i+1/2,j+1/2,-1/2} = u_{i+1/2,j+1/2,1/2} + O(h^5), \quad u_{i+1/2,j+1/2,-3/2} = u_{i+1/2,j+1/2,3/2} + O(h^5). \tag{2.11}$$

Similar extrapolation formulas could be derived to two other components, namely v and w, and we arrive at the boundary condition for the numerical scheme (2.4):

$$\mathbf{u}^{n+1}_{i+1/2,j+1/2,-1/2} = \mathbf{u}^{n+1}_{i+1/2,j+1/2,1/2}, \quad \mathbf{u}^{n+1}_{i+1/2,j+1/2,-3/2} = \mathbf{u}^{n+1}_{i+1/2,j+1/2,3/2}. \tag{2.12}$$

Analogous formulas follow for the remaining three boundaries. The stability of the above one-sided approximations near the boundary will be proved in later sections; also see the related works [20–24].

Similarly, a fourth order accurate (in time) numerical scheme could be derived as follows, which combines the Adams–Bashforth explicit extrapolation (for the nonlinear terms) and the Adams–Mouton interpolation (for the diffusion term):

$$\begin{aligned}&\frac{\mathbf{u}^{n+1}-\mathbf{u}^n}{\Delta t}-\Delta_{h,(4)}\Big(\frac{757}{1152}\mathbf{u}^{n+1}+\frac{470}{1152}\mathbf{u}^{n-1}-\frac{118}{1152}\mathbf{u}^{n-5}+\frac{43}{1152}\mathbf{u}^{n-7}\Big)\\ =&\frac{55}{24}|\nabla_{h,(4)}\mathbf{u}^n|^2\mathbf{u}^n-\frac{59}{24}|\nabla_{h,(4)}\mathbf{u}^{n-1}|^2\mathbf{u}^{n-1}+\frac{37}{24}|\nabla_{h,(4)}\mathbf{u}^{n-2}|^2\mathbf{u}^{n-2}-\frac{3}{8}|\nabla_{h,(4)}\mathbf{u}^{n-3}|^2\mathbf{u}^{n-3}.\end{aligned}\tag{2.13}$$

To carry out the stability and convergence analysis, we have to introduce a discrete ℓ^2 inner product and ℓ^2 norm:

$$\|\mathbf{f}\|_2=\sqrt{\langle\mathbf{f},\mathbf{f}\rangle},\quad\text{with}\quad\langle\mathbf{f},\mathbf{g}\rangle=h^3\sum_{i,j,k=0}^{N-1}f_{i+1/2,j+1/2,k+1/2}g_{i+1/2,j+1/2,k+1/2},\tag{2.14}$$

for all grid functions $\mathbf{f}$, $\mathbf{g}$ evaluated on staggered mesh points. In particular, the discrete inner product of two discrete gradient vectors is defined as

$$\langle\nabla_h\mathbf{f},\nabla_h\mathbf{g}\rangle=\langle D_x\mathbf{f},D_x\mathbf{g}\rangle+\langle D_y\mathbf{f},D_y\mathbf{g}\rangle+\langle D_z\mathbf{f},D_z\mathbf{g}\rangle,\quad\|\nabla_h\mathbf{f}\|_2=\sqrt{\langle\nabla_h\mathbf{f},\nabla_h\mathbf{f}\rangle},\tag{2.15}$$

$$\langle D_x\mathbf{f},D_x\mathbf{g}\rangle=h^3\sum_{i,k=0}^{N-1}\Big(\sum_{i=0}^{N}a_i(D_xf)_{i,j+1/2,k+1/2}(D_xg)_{i,j+1/2,k+1/2}\Big),$$

$$\langle D_y\mathbf{f},D_y\mathbf{g}\rangle=h^3\sum_{j,k=0}^{N-1}\Big(\sum_{j=0}^{N}a_j(D_xf)_{i+1/2,j,k+1/2}(D_xg)_{i+1/2,j,k+1/2}\Big),$$

$$\langle D_z\mathbf{f},D_z\mathbf{g}\rangle=h^3\sum_{i,j=0}^{N-1}\Big(\sum_{k=0}^{N}a_k(D_zf)_{i+1/2,j+1/2,k}(D_zg)_{i+1/2,j+1/2,k}\Big),$$

with $a_0=a_N=0$, and $a_j=1$ for $1\le j\le N-1$. Notice that the homogeneous Neumann boundary condition is imposed for $\mathbf{f}$ and $\mathbf{g}$, as given by (2.12), in the evaluation of their discrete gradient. In addition, the following summation by parts formulas will be used in the later analysis:

$$-\langle\mathbf{f},\Delta_h^2\mathbf{g}\rangle=\langle\nabla_h\mathbf{f},\nabla_h\mathbf{g}\rangle,\ \ \langle\mathbf{f},D_x^4\mathbf{g}\rangle=\langle D_x^2\mathbf{f},D_x^2\mathbf{g}\rangle,\ \ \langle\mathbf{f},D_y^4\mathbf{g}\rangle=\langle D_y^2\mathbf{f},D_y^2\mathbf{g}\rangle,\ \ \langle\mathbf{f},D_z^4\mathbf{g}\rangle=\langle D_z^2\mathbf{f},D_z^2\mathbf{g}\rangle,\tag{2.16}$$

with $\mathbf{f}$ and $\mathbf{g}$ satisfying homogeneous Neumann boundary condition given by (2.12). Furthermore, the following estimate is needed in the later stability and convergence analysis.

Lemma 2.1. *For $\mathbf{f}$ and $\mathbf{g}$ satisfying homogeneous Neumann boundary condition given by (2.12), we have*

$$\begin{aligned}-\langle\mathbf{f},\Delta_{h,(4)}\mathbf{g}\rangle&=\langle\nabla_h\mathbf{f},\nabla_h\mathbf{g}\rangle_{(4)}\\&=\langle\nabla_h\mathbf{f},\nabla_h\mathbf{g}\rangle+\frac{h^2}{12}(\langle D_x^2\mathbf{f},D_x^2\mathbf{g}\rangle+\langle D_y^2\mathbf{f},D_y^2\mathbf{g}\rangle+\langle D_z^2\mathbf{f},D_z^2\mathbf{g}\rangle).\end{aligned}\tag{2.17}$$

Proof. Because of the fact that $\mathcal{D}_{x,(4)}^2\mathbf{g}=(D_x^2-\frac{h^2}{12}D_x^4)\mathbf{g}$ (and similar definitions for $\mathcal{D}_{x,(4)}^2$ and $\mathcal{D}_{y,(4)}^2$), the estimate (2.17) is a direct consequences of the following identities, which come from an application of the summation by parts formulas (2.16):

$$-\langle\mathbf{f},\mathcal{D}_{x,(4)}^2\mathbf{g}\rangle=\langle D_x\mathbf{f},D_x\mathbf{g}\rangle+\frac{h^2}{12}\langle D_x^2\mathbf{f},D_x^2\mathbf{g}\rangle,\quad-\langle\mathbf{f},\mathcal{D}_{y,(4)}^2\mathbf{g}\rangle=\langle D_y\mathbf{f},D_y\mathbf{g}\rangle+\frac{h^2}{12}\langle D_y^2\mathbf{f},D_y^2\mathbf{g}\rangle,$$

$$-\langle\mathbf{f},\mathcal{D}_{z,(4)}^2\mathbf{g}\rangle=\langle D_z\mathbf{f},D_z\mathbf{g}\rangle+\frac{h^2}{12}\langle D_z^2\mathbf{f},D_z^2\mathbf{g}\rangle.\quad\square$$

In turn, for any $\mathbf{f}$ satisfying the homogeneous boundary condition given by (2.12), we introduce the following auxiliary norms, which will facilitate the later analysis.

$$\|\nabla_h\mathbf{f}\|_{2,(4)}:=\Big(\|\nabla_h\mathbf{f}\|_2^2+\frac{h^2}{12}(\|D_x^2\mathbf{f}\|_2^2+\|D_y^2\mathbf{f}\|_2^2+\|D_z^2\mathbf{f}\|_2^2)\Big)^{\frac12}.\tag{2.18}$$

As a result, an application of Cauchy inequality yields the following result, in combination with (2.17):

$$\big|\langle\nabla_h\mathbf{f},\nabla_h\mathbf{g}\rangle_{(4)}\big|\le\|\nabla_h\mathbf{f}\|_{2,(4)}\cdot\|\nabla_h\mathbf{g}\|_{2,(4)}\le\frac12(\|\nabla_h\mathbf{f}\|_{2,(4)}^2+\|\nabla_h\mathbf{g}\|_{2,(4)}^2).\tag{2.19}$$

In addition, the following estimates are needed in the later analysis.

Lemma 2.2. *For* $\mathbf{f}$ *satisfying homogeneous Neumann boundary condition given by (2.12), we have*

$$\|\nabla_h \mathbf{f}\|_2 \le \|\nabla_h \mathbf{f}\|_{2,(4)}, \tag{2.20}$$

$$\|\nabla_{h,(4)} \mathbf{f}\|_2^2 \le \frac{25}{9}\|\nabla_h \mathbf{f}\|_2^2, \quad \text{with } \|\nabla_{h,(4)} \mathbf{f}\|_2^2 := \|\mathcal{D}^1_{x,(4)} \mathbf{f}\|_2^2 + \|\mathcal{D}^1_{y,(4)} \mathbf{f}\|_2^2 + \|\mathcal{D}^1_{z,(4)} \mathbf{f}\|_2^2. \tag{2.21}$$

Proof. Inequality (2.20) comes directly from the definition (2.18). For the inequality (2.21), we begin with the following observation (based on the definition (2.1):

$$\mathcal{D}^1_{x,(4)} \mathbf{f}_{i+1/2} = -\frac{1}{12}(D_x \mathbf{f})_{i-1} + \frac{7}{12}(D_x \mathbf{f})_i + \frac{7}{12}(D_x \mathbf{f})_{i+1} - \frac{1}{12}(D_x \mathbf{f})_{i+2}. \tag{2.22}$$

In turn, an application of the Cauchy inequality implies that

$$\left|\mathcal{D}^1_{x,(4)} \mathbf{f}_{i+1/2}\right|^2 \le 4\Big(\frac{1}{12^2}((D_x \mathbf{f})^2_{i-1} + D_x \mathbf{f})^2_{i+2} + \frac{7^2}{12^2}((D_x \mathbf{f})^2_i + (D_x \mathbf{f})^2_{i+1})\Big). \tag{2.23}$$

Summing over index i, we get

$$\|\mathcal{D}^1_{x,(4)} \mathbf{f}\|_2^2 \le 4\Big(2 \cdot \frac{1}{12^2} + 2 \cdot \frac{7^2}{12^2}\Big)\|D_x \mathbf{f}\|_2^2 = \frac{25}{9}\|D_x \mathbf{f}\|_2^2. \tag{2.24}$$

Similar estimate could be derived for $\|\mathcal{D}^1_{y,(4)} \mathbf{f}\|_2^2$ and $\|\mathcal{D}^1_{z,(4)} \mathbf{f}\|_2^2$:

$$\|\mathcal{D}^1_{y,(4)} \mathbf{f}\|_2^2 \le \frac{25}{9}\|D_y \mathbf{f}\|_2^2, \quad \|\mathcal{D}^1_{z,(4)} \mathbf{f}\|_2^2 \le \frac{25}{9}\|D_z \mathbf{f}\|_2^2. \tag{2.25}$$

Finally, inequality (2.21) is a direct consequence of (2.24) and (2.25). □

In addition to the standard ℓ^2 norm, we also introduce the ℓ^p, $1 \le p < \infty$, and ℓ^∞ norms for a grid function $f \in \mathcal{G}_N$:

$$\|f\|_\infty := \max_{i,j,k} |f_{i+1/2,j+1/2,k+1/2}|, \qquad \|f\|_p := \Big(h^3 \sum_{i,j,k=0}^{N-1} |f_{i+1/2,j+1/2,k+1/2}|^p\Big)^{\frac{1}{p}}, \quad 1 \le p < \infty. \tag{2.26}$$

The main theoretical result of this article is stated below.

Theorem 2.3. *For any time* $T^* > 0$*, we assume that exact solution* $\mathbf{u}_e$ *to the harmonic mapping flow equation (1.2) satisfies the regularity requirement* $\mathbf{u}_e \in H^3(0, T; H^3) \cap L^\infty(0, T; H^6)$*. We denote the* $\mathbf{u}_{\Delta t,h}$ *as the continuous function as the extension of the fully discrete numerical solution obtained by (2.4). As* $\Delta t, h \to 0$ *under a linear refinement requirement* $\Delta t \le Ch$*, we obtain the following result:*

$$\|\mathbf{u}_{\Delta t,h} - \mathbf{u}_e\|_{\ell^\infty(0,T^*;\ell^2)} + \|\mathbf{u}_{\Delta t,h} - \mathbf{u}_e\|_{\ell^2(0,T^*;H_h^1)} \le C(\Delta t^3 + h^4). \tag{2.27}$$

In the later sections, we denote $\mathbf{u}$ and $\mathbf{U}$ as the numerical solution and the exact solution, respectively.

3. The convergence analysis

3.1. The consistency analysis

We denote $\mathbf{U} = \mathbf{u}_e$ as the exact solution, and make a symmetric extension at the "ghost" numerical mesh points (around the boundary section $\Gamma_z : z = 0$):

$$\mathbf{U}_{i+1/2,j+1/2,-1/2} = \mathbf{U}_{i+1/2,j+1/2,1/2}, \quad \mathbf{U}_{i+1/2,j+1/2,-3/2} = \mathbf{U}_{i+1/2,j+1/2,3/2}. \tag{3.1}$$

The following truncation error estimates can be derived using a high order Taylor expansion in time:

$$\mathbf{U}^{n+1} - \mathbf{U}^n = \int_{t^n}^{t^{n+1}} \partial_t \mathbf{U}(\cdot, t)\, dt,$$

$$\frac{23}{12}|\nabla \mathbf{U}^n|^2 \mathbf{U}^n - \frac{4}{3}|\nabla \mathbf{U}^{n-1}|^2 \mathbf{U}^{n-1} + \frac{5}{12}|\nabla \mathbf{U}^{n-2}|^2 \mathbf{U}^{n-2} = \frac{1}{\Delta t}\int_{t^n}^{t^{n+1}} |\nabla \mathbf{U}|^2 \mathbf{U}(\cdot, t)\, dt + \boldsymbol{\tau}_1^n,$$

$$\text{with } \|\boldsymbol{\tau}_1\|_{\ell^2(0,T^*;L^2)} \le C\Delta t^3 \|\mathbf{U}\|^2_{H^3(0,T^*;H^3)} \le C\Delta t^3,$$

$$\Delta\Big(\frac{2}{3}\mathbf{U}^{n+1} + \frac{5}{12}\mathbf{U}^{n-1} - \frac{1}{12}\mathbf{U}^{n-3}\Big) = \frac{1}{\Delta t}\int_{t^n}^{t^{n+1}} \Delta \mathbf{U}(\cdot, t)\, dt + \boldsymbol{\tau}_2^n,$$

$$\text{with } \|\boldsymbol{\tau}_2\|_{\ell^2(0,T^*;L^2)} \le C\Delta t^3 \|\mathbf{U}_N\|_{H^3(0,T^*;H^2)} \le C\Delta t^3.$$

This in turn leads to the third order temporal consistency of the approximate solution $\mathbf{U}$:

$$\frac{\mathbf{U}^{n+1}-\mathbf{U}^n}{\Delta t}-\frac{23}{12}|\nabla\mathbf{U}^n|^2\mathbf{U}^n+\frac{4}{3}|\nabla\mathbf{U}^{n-1}|^2\mathbf{U}^{n-1}-\frac{5}{12}|\nabla\mathbf{U}^{n-2}|^2\mathbf{U}^{n-2}$$
$$-\Delta\left(\frac{2}{3}\mathbf{U}^{n+1}+\frac{5}{12}\mathbf{U}^{n-1}-\frac{1}{12}\mathbf{U}^{n-3}\right)=\boldsymbol{\tau}_3^n, \tag{3.2}$$

with $\|\boldsymbol{\tau}_3\|_{\ell^2(0,T^*;\ell^2)}\le C\Delta t^3$. Meanwhile, by making use of the consistency analysis for the long stencil difference approximation, established in a recent work [24], we have

$$\|\nabla\mathbf{U}^n-\nabla_{h,(4)}\mathbf{U}^n\|_2\le Ch^4\|\mathbf{U}\|_{H^5},\quad \|\Delta\mathbf{U}^n-\Delta_{h,(4)}\mathbf{U}^n\|_2\le Ch^4\|\mathbf{U}\|_{H^6}. \tag{3.3}$$

Note that such an approximation estimate was derived in [24] based on the periodic boundary condition, which this analysis could also be applied to the test function with homogeneous Neumann boundary condition. This in turn leads to the spatial truncation error estimate for the numerical scheme:

$$|\nabla\mathbf{U}^k|^2\mathbf{U}^k-|\nabla_{h,(4)}\mathbf{U}^k|^2\mathbf{U}^k=O(h^4)\|\mathbf{U}^k\|_{H^5}\cdot\|\mathbf{U}^k\|_{H^3}^2,\quad \Delta_{h,(4)}\mathbf{U}^k-\Delta\mathbf{U}^k=O(h^4)\|\mathbf{U}^k\|_{H^6}, \tag{3.4}$$

for $k=n,n-1,n-2,n-3$. A combination of (3.2) and (3.4) yields the desired consistency estimate for the fully discrete scheme, with third order temporal accuracy order and fourth order spatial accuracy order:

$$\frac{\mathbf{U}^{n+1}-\mathbf{U}^n}{\Delta t}-\frac{23}{12}|\nabla_{h,(4)}\mathbf{U}^n|^2\mathbf{U}^n+\frac{4}{3}|\nabla_{h,(4)}\mathbf{U}^{n-1}|^2\mathbf{U}^{n-1}-\frac{5}{12}|\nabla_{h,(4)}\mathbf{U}^{n-2}|^2\mathbf{U}^{n-2}$$
$$=\Delta_{h,(4)}\left(\frac{2}{3}\mathbf{U}^{n+1}+\frac{5}{12}\mathbf{U}^{n-1}-\frac{1}{12}\mathbf{U}^{n-3}\right)+\boldsymbol{\tau}^n,\quad \text{with } \|\boldsymbol{\tau}\|_{\ell^2(0,T^*;\ell^2)}\le C\left(\Delta t^3+h^4\right). \tag{3.5}$$

In addition, we have to establish the discrete boundary condition for the exact solution, analogous to (2.12). For simplicity, we focus on the u_e component, and this analysis could be extended to the two other components in a straightforward way. First, a higher order Taylor expansion around $\Gamma_z: z=0$ gives

$$(u_e)_{i+1/2,j+1/2,-1/2}=(u_e)_{i+1/2,j+1/2,1/2}-h(\partial_z u_e)_{i+1/2,j+1/2,0}-\frac{h^3}{24}(\partial_z^3 u_e)_{i+1/2,j+1/2,0}$$
$$-\frac{h^5}{1920}(\partial_z^5 u_e)_{i+1/2,j+1/2,0}+O(h^7), \tag{3.6}$$
$$(u_e)_{i+1/2,j+1/2,-3/2}=(u_e)_{i+1/2,j+1/2,3/2}-3h(\partial_z u_e)_{i+1/2,j+1/2,0}-\frac{9h^3}{8}(\partial_z^3 u_e)_{i+1/2,j+1/2,0}$$
$$-\frac{81h^5}{640}(\partial_z^5 u_e)_{i+1/2,j+1/2,0}+O(h^7). \tag{3.7}$$

Meanwhile, we have to perform similar analysis as in the derivations in (2.7)–(2.10) to obtain an exact value of $\partial_z^5 u_e$ along Γ_z. An application of ∂_z^3 operator to the first evolutionary equation in (1.2) along Γ_z, as well as careful boundary evaluations, will result in the following boundary condition for $\partial_z^5 u_e$:

$$\partial_z^5 u_e=0,\quad \text{on } \Gamma_z. \tag{3.8}$$

The details are skipped for the sake of brevity. Therefore, a substitution of (3.8) into (3.6), (3.7) results in the higher order extrapolation estimates:

$$(u_e)_{i+1/2,j+1/2,-1/2}=(u_e)_{i+1/2,j+1/2,1/2}+O(h^7),$$
$$(u_e)_{i+1/2,j+1/2,-3/2}=(u_e)_{i+1/2,j+1/2,3/2}+O(h^7). \tag{3.9}$$

The same estimates are also available for the components v_e and w_e. In comparison with the exact extrapolation formula (3.1), we see that the $O(h^7)$ extrapolation error does not cause an $O(h^4)$ accuracy order loss (for the spatial discretization) around the boundary points.

Subsequently, the numerical error function is defined at a point-wise level:

$$\boldsymbol{e}^k=\mathbf{U}^k-\mathbf{u}^k,\quad \forall k\ge 0. \tag{3.10}$$

In turn, subtracting the numerical scheme (2.4) from the consistency estimate (3.5) gives

$$\frac{\boldsymbol{e}^{n+1}-\boldsymbol{e}^n}{\Delta t}-\frac{23}{12}\mathcal{NLE}^n+\frac{4}{3}\mathcal{NLE}^{n-1}-\frac{5}{12}\mathcal{NLE}^{n-2}$$
$$=\Delta_{h,(4)}\left(\frac{2}{3}\boldsymbol{e}^{n+1}+\frac{5}{12}\boldsymbol{e}^{n-1}-\frac{1}{12}\boldsymbol{e}^{n-3}\right)+\boldsymbol{\tau}^n, \tag{3.11}$$
$$\text{with } \mathcal{NLE}^k=|\nabla_{h,(4)}\mathbf{u}^k|^2\boldsymbol{e}^k+\left(\nabla_{h,(4)}(\mathbf{U}^k+\mathbf{u}^k)\otimes\nabla_{h,(4)}\boldsymbol{e}^k\right)\mathbf{U}^k,\quad k=n,n-1,n-2. \tag{3.12}$$

Furthermore, by the boundary extrapolation formula (2.12) and the estimate (3.9), we conclude that

$$\boldsymbol{e}_{i+1/2,j+1/2,-1/2} = \boldsymbol{e}_{i+1/2,j+1/2,1/2}, \quad \boldsymbol{e}_{i+1/2,j+1/2,-3/2} = \boldsymbol{e}_{i+1/2,j+1/2,3/2}. \tag{3.13}$$

The exact solution has a discrete $W^{2,\infty}$ bound

$$\|\mathbf{U}\|_{L^\infty(0,T^*;W_h^{1,\infty})} \le C^*, \quad \text{i.e. } \|\mathbf{U}^k\|_\infty \le C^*, \ \|\nabla_h \mathbf{U}^k\|_\infty \le C^*, \tag{3.14}$$

for any $k \ge 0$, which comes from the regularity of the constructed solution. Furthermore, making use of the detailed expansion (2.22) for the $\mathcal{D}^1_{x,(4)}$ operator, we get the following bound for the exact solution:

$$\|\nabla_{h,(4)} \mathbf{U}^k\|_\infty \le \frac{4}{3}\|\nabla_h \mathbf{U}^k\|_\infty \le \frac{4}{3} C^*, \quad \text{for any } k. \tag{3.15}$$

3.2. An a-priori $W_h^{1,\infty}$ assumption

We assume a-priori that the numerical error function has a $W_h^{1,\infty}$ bound at the previous time steps:

$$\|\boldsymbol{e}^k\|_\infty \le 1, \quad \|\nabla_h \boldsymbol{e}^k\|_\infty \le 1, \quad \text{with } k = n, n-1, n-2, \tag{3.16}$$

so that the $W_h^{1,\infty}$ bound for the numerical solution at these time steps can be obtained as

$$\begin{aligned} &\|\mathbf{u}^k\|_\infty = \|\mathbf{U}^k - \boldsymbol{e}^k\|_\infty \le \|\mathbf{U}^k\|_\infty + \|\boldsymbol{e}^k\|_\infty \le C^* + 1 := \tilde{C}_0, \\ &\|\nabla_h \mathbf{u}^k\|_\infty = \|\nabla_h \mathbf{U}^k - \nabla_h \boldsymbol{e}^k\|_\infty \le \|\nabla_h \mathbf{U}^k\|_\infty + \|\nabla_h \boldsymbol{e}^k\|_\infty \le C^* + 1 = \tilde{C}_0. \end{aligned} \tag{3.17}$$

Similarly, we are able to derive the following bound for the numerical solution, based on the detailed expansion (2.22):

$$\|\nabla_{h,(4)} \mathbf{u}^k\|_\infty \le \frac{4}{3}\|\nabla_h \mathbf{u}^k\|_\infty \le \frac{4}{3}\tilde{C}_0, \quad \text{for } k = n, n-1, n-2. \tag{3.18}$$

Such a $W_h^{1,\infty}$ assumption (3.16) for the numerical error function could be recovered at the next time step, via the ℓ^2 convergence estimate, combined with an application of inverse inequality, as will be demonstrated in the later analysis.

3.3. The $\ell^\infty(0,T^*;\ell^2) \cap \ell^2(0,T^*;H_h^1)$ error estimate

Taking a discrete ℓ^2 inner product of (3.11) with $2\boldsymbol{e}^{n+1}$ yields

$$\begin{aligned} &\left\langle \boldsymbol{e}^{n+1} - \boldsymbol{e}^n, 2\boldsymbol{e}^{n+1} \right\rangle - \Delta t \left\langle \Delta_{h,(4)} \left(\frac{4}{3}\boldsymbol{e}^{n+1} + \frac{5}{6}\boldsymbol{e}^{n-1} - \frac{1}{6}\boldsymbol{e}^{n-3} \right), \boldsymbol{e}^{n+1} \right\rangle \\ &= \frac{23}{6}\Delta t \left\langle \mathcal{NLE}^n, \boldsymbol{e}^{n+1} \right\rangle - \frac{8}{3}\Delta t \left\langle \mathcal{NLE}^{n-1}, \boldsymbol{e}^{n+1} \right\rangle + \frac{5}{6}\Delta t \left\langle \mathcal{NLE}^{n-2}, \boldsymbol{e}^{n+1} \right\rangle + 2\Delta t \left\langle \boldsymbol{\tau}^n, \boldsymbol{e}^{n+1} \right\rangle. \end{aligned} \tag{3.19}$$

The time marching term and the truncation error term can be handled in a straightforward way:

$$\left\langle \boldsymbol{e}^{n+1} - \boldsymbol{e}^n, 2\boldsymbol{e}^{n+1} \right\rangle = \left\| \boldsymbol{e}^{n+1} \right\|_2^2 - \left\| \boldsymbol{e}^n \right\|_2^2 + \left\| \boldsymbol{e}^{n+1} - \boldsymbol{e}^n \right\|_2^2, \tag{3.20}$$

$$2\left\langle \boldsymbol{\tau}^n, \boldsymbol{e}^{n+1} \right\rangle \le \left\| \boldsymbol{\tau}^n \right\|_2^2 + \left\| \boldsymbol{e}^{n+1} \right\|_2^2, \tag{3.21}$$

in which a discrete Cauchy inequality was utilized. For the diffusion part, we see that the diffusion coefficient at t^{n+1} dominates the other ones, so that the viscosity term can be analyzed in the same way as follows:

$$\begin{aligned} &-\left\langle \Delta_{h,(4)} \left(\frac{4}{3}\boldsymbol{e}^{n+1} + \frac{5}{6}\boldsymbol{e}^{n-1} - \frac{1}{6}\boldsymbol{e}^{n-3} \right), \boldsymbol{e}^{n+1} \right\rangle \\ &= \frac{4}{3}\|\nabla_h \boldsymbol{e}^{n+1}\|_{2,(4)}^2 + \frac{5}{6}\langle \nabla_h \boldsymbol{e}^{n-1}, \nabla_h \boldsymbol{e}^{n+1} \rangle_{(4)} - \frac{1}{6}\langle \nabla_h \boldsymbol{e}^{n-3}, \nabla_h \boldsymbol{e}^{n+1} \rangle_{(4)} \\ &\ge \frac{4}{3}\|\nabla_h \boldsymbol{e}^{n+1}\|_{2,(4)}^2 - \frac{5}{12}(\|\nabla_h \boldsymbol{e}^{n-1}\|_{2,(4)}^2 + \|\nabla_h \boldsymbol{e}^{n+1}\|_{2,(4)}^2) - \frac{1}{12}(\|\nabla_h \boldsymbol{e}^{n-3}\|_{2,(4)}^2 + \|\nabla_h \boldsymbol{e}^{n+1}\|_{2,(4)}^2) \\ &\ge \frac{5}{6}\|\nabla_h \boldsymbol{e}^{n+1}\|_{2,(4)}^2 - \frac{5}{12}\|\nabla_h \boldsymbol{e}^{n-1}\|_{2,(4)}^2 - \frac{1}{12}\|\nabla_h \boldsymbol{e}^{n-3}\|_{2,(4)}^2, \end{aligned} \tag{3.22}$$

in which the equality (2.17) (in Lemma 2.1) and the estimate (2.19) have been repeatedly applied in the derivation.

For the nonlinear error parts, we focus on the term $\mathcal{NLE}^n$; the two other terms could be treated in the same manner. The nonlinear error expansion (3.12) implies that

$$\langle \mathcal{NLE}^n, \boldsymbol{e}^{n+1} \rangle = \langle |\nabla_{h,(4)} \mathbf{u}^n|^2 \boldsymbol{e}^n, \boldsymbol{e}^{n+1} \rangle + \left\langle \left(\nabla_{h,(4)} (\mathbf{U}^n + \mathbf{u}^n) \otimes \nabla_{h,(4)} \boldsymbol{e}^n \right) \mathbf{U}^n, \boldsymbol{e}^{n+1} \right\rangle. \tag{3.23}$$

The first term could be bounded with the help of the a-priori bound (3.18) (a direct consequence of the a-priori assumption (3.16)):

$$\begin{aligned}\langle|\nabla_{h,(4)}\mathbf{u}^n|^2\boldsymbol{e}^n,\boldsymbol{e}^{n+1}\rangle &\le \|\nabla_{h,(4)}\mathbf{u}^n\|_\infty^2\cdot\|\boldsymbol{e}^n\|_2\cdot\|\boldsymbol{e}^{n+1}\|_2\\ &\le (\frac{4}{3}\tilde{C}_0)^2\|\boldsymbol{e}^n\|_2\cdot\|\boldsymbol{e}^{n+1}\|_2\le\frac{8}{9}\tilde{C}_0^2(\|\boldsymbol{e}^n\|_2^2+\|\boldsymbol{e}^{n+1}\|_2^2).\end{aligned}\tag{3.24}$$

The second term could be similarly bounded, with the help of both (3.15) and (3.18):

$$\begin{aligned}&\left\langle\left(\nabla_{h,(4)}(\mathbf{U}^n+\mathbf{u}^n)\otimes\nabla_{h,(4)}\boldsymbol{e}^n\right)\mathbf{U}^n,\boldsymbol{e}^{n+1}\right\rangle\\ &\le(\|\nabla_{h,(4)}\mathbf{U}^n\|_\infty+\|\nabla_{h,(4)}\mathbf{u}^n\|_\infty)\cdot\|\mathbf{U}^n\|_\infty\cdot\|\nabla_{h,(4)}\boldsymbol{e}^n\|_2\cdot\|\boldsymbol{e}^{n+1}\|_2\\ &\le\frac{4}{3}C^*(\tilde{C}_0+C^*)\|\nabla_{h,(4)}\boldsymbol{e}^n\|_2\cdot\|\boldsymbol{e}^{n+1}\|_2\le\frac{20}{9}C^*(\tilde{C}_0+C^*)\|\nabla_h\boldsymbol{e}^n\|_2\cdot\|\boldsymbol{e}^{n+1}\|_2,\end{aligned}\tag{3.25}$$

in which the inequality estimate (2.21) has been applied in the last step. Therefore, a substitution of (3.24) and (3.25) into (3.23) reveals that

$$\begin{aligned}\frac{23}{6}\langle\mathcal{NLE}^n,\boldsymbol{e}^{n+1}\rangle &\le\frac{92}{27}\tilde{C}_0^2(\|\boldsymbol{e}^n\|_2^2+\|\boldsymbol{e}^{n+1}\|_2^2)+\frac{230}{27}C^*(\tilde{C}_0+C^*)\|\nabla_h\boldsymbol{e}^n\|_2\cdot\|\boldsymbol{e}^{n+1}\|_2\\ &\le\tilde{C}_1\|\boldsymbol{e}^n\|_2^2+\tilde{C}_2\|\boldsymbol{e}^{n+1}\|_2^2+\frac{1}{12}\|\nabla_h\boldsymbol{e}^n\|_2^2,\end{aligned}\tag{3.26}$$

with $\tilde{C}_1=\frac{92}{27}\tilde{C}_0^2$, $\tilde{C}_2=\frac{92}{27}\tilde{C}_0^2+\frac{230^2}{243}(C^*)^2(\tilde{C}_0+C^*)^2$, and the Cauchy inequality has been applied in the last step. Similar estimate could be derived for the two other nonlinear error parts; the details are skipped for the sake of brevity.

$$-\frac{8}{3}\langle\mathcal{NLE}^{n-1},\boldsymbol{e}^{n+1}\rangle\le\tilde{C}_1\|\boldsymbol{e}^{n-1}\|_2^2+\tilde{C}_2\|\boldsymbol{e}^{n+1}\|_2^2+\frac{1}{12}\|\nabla_h\boldsymbol{e}^{n-1}\|_2^2,\tag{3.27}$$

$$\frac{5}{6}\langle\mathcal{NLE}^{n-2},\boldsymbol{e}^{n+1}\rangle\le\tilde{C}_1\|\boldsymbol{e}^{n-2}\|_2^2+\tilde{C}_2\|\boldsymbol{e}^{n+1}\|_2^2+\frac{1}{12}\|\nabla_h\boldsymbol{e}^{n-2}\|_2^2.\tag{3.28}$$

Subsequently, a substitution of (3.20)–(3.21), (3.22), (3.26)–(3.28) into (3.19) results in

$$\begin{aligned}&\left\|\boldsymbol{e}^{n+1}\right\|_2^2-\left\|\boldsymbol{e}^n\right\|_2^2+\frac{5}{6}\Delta t\|\nabla_h\boldsymbol{e}^{n+1}\|_{2,(4)}^2-\frac{1}{12}\Delta t\|\nabla_h\boldsymbol{e}^n\|_{2,(4)}^2-\frac{1}{2}\Delta t\|\nabla_h\boldsymbol{e}^{n-1}\|_{2,(4)}^2\\ &\quad-\frac{1}{12}\Delta t\left(\|\nabla_h\boldsymbol{e}^{n-2}\|_{2,(4)}^2+\|\nabla_h\boldsymbol{e}^{n-3}\|_{2,(4)}^2\right)\\ &\le(3\tilde{C}_2+1)\Delta t\|\boldsymbol{e}^{n+1}\|_2^2+\tilde{C}_1\Delta t\left(\|\boldsymbol{e}^n\|_2^2+\|\boldsymbol{e}^{n-1}\|_2^2+\|\boldsymbol{e}^{n-2}\|_2^2\right)+\Delta t\|\boldsymbol{\tau}^n\|_2^2,\end{aligned}\tag{3.29}$$

in which the preliminary estimate (2.20) has been applied. Consequently, summing in time, applying the discrete Gronwall inequality and using a simple fact that $\frac{5}{6}-\frac{3}{12}-\frac{1}{2}=\frac{1}{12}>0$, we get a fixed time $O(\Delta t^3+h^m)$ convergence for the third order scheme (2.4) in the $\ell^\infty(0,T^*;\ell^2)\cap\ell^2(0,T^*;H_h^1)$ norm:

$$\|\boldsymbol{e}^{n+1}\|_2^2+\frac{1}{12}\Delta t\sum_{k=1}^{n+1}\|\nabla_h\boldsymbol{e}^k\|_2^2\le\tilde{C}_3\left(\Delta t^3+h^m\right)^2,\tag{3.30}$$

under the a-priori $W_h^{1,\infty}$ assumption (3.16). Again, the preliminary estimate (2.20) has been applied.

3.4. Recovery of the a-priori $W_h^{1,\infty}$ bound (3.16)

Finally, with the help of the ℓ^2 error estimate (3.30), an application of the inverse inequality (in 3-D) implies that

$$\|\nabla\boldsymbol{e}^{n+1}\|_\infty\le\frac{C\|\boldsymbol{e}^{n+1}\|_2}{h^{\frac{3}{2}}}\le\frac{C\tilde{C}_3^{\frac{1}{2}}(\Delta t^3+h^4)}{h^{\frac{3}{2}}}\le\hat{C}_1\tilde{C}_3^{\frac{1}{2}}(\Delta t^{\frac{3}{2}}+h^{\frac{5}{2}}),\tag{3.31}$$

$$\|\nabla_h\boldsymbol{e}^{n+1}\|_\infty\le\frac{C\|\boldsymbol{e}^{n+1}\|_\infty}{h}\le\frac{C\tilde{C}_3^{\frac{1}{2}}(\Delta t^{\frac{3}{2}}+h^{\frac{5}{2}})}{h^{\frac{3}{2}}}\le\hat{C}_2\tilde{C}_3^{\frac{1}{2}}(\Delta t^{\frac{1}{2}}+h^{\frac{3}{2}}),\tag{3.32}$$

in which we have used the linear refinement $\Delta t\le Ch$ in the derivation. As a result, we see that the a-priori $W_h^{1,\infty}$ bound (3.16) is also valid for the numerical error vector $\boldsymbol{e}^{n+1}$ at time step t^{n+1} provided that

$$\Delta t\le\left(2\hat{C}_1\tilde{C}_3^{\frac{1}{2}}\right)^{-2},\quad h\le\left(2\hat{C}_2\tilde{C}_3^{\frac{1}{2}}\right)^{-\frac{2}{3}},\quad\text{with }\tilde{C}_3\text{ dependent on }T^*.\tag{3.33}$$

This completes the $\ell^\infty(0,T^*;\ell^2)\cap\ell^2(0,T^*;H_h^1)$ convergence analysis, and the proof of Theorem 2.3.

Remark 3.1. Since the leading order Taylor expansion has already resulted in an $O(\Delta t^3+h^4)$ accuracy order, it is sufficient to control the discrete $W_h^{1,\infty}$ bound of the numerical error function, as derived in (3.31), (3.32). As a result, we do not need a higher order asymptotic expansion in the consistency analysis, in contrast to a few other related works [41–46].

Remark 3.2. It is observed that, the diffusion coefficient at time step t^{n+1} dominates the rest coefficient sum. This fact has played a key role in the stability and convergence estimate; also see the related discussions in [26,27]. In fact, to derive a temporally third order accurate numerical scheme, a direct application of the Adams–Moulton formula at the nodes t^{n+1}, t^n and t^{n-1} does not give a formula with the stated stability property. This fact highlights the need to choose an appropriate time-discretization to couple with the fourth order finite difference spatial approximation.

Remark 3.3. For the harmonic mapping flow (1.2), there is a well-known property that, $|\mathbf{u}(\mathbf{x},t)| = 1$ holds for any $t>0$, provided that the initial data satisfies $|\mathbf{u}(\mathbf{x},t=0)|=1$ at a point-wise level. However, for the proposed numerical scheme (2.4), such a property is not valid any more, because of the temporal and spatial discretization. Meanwhile, the convergence estimate (stated in Theorem 2.3) implies that, although such an identity is not exactly available, the deviation is always of order $O(\Delta t^3+h^4)$ (in the discrete L^2 average sense).

3.5. The fourth order convergence result

For the fourth order accurate (in time) scheme (2.13), the convergence estimate is stated below. It proof follows similar ideas as in the analysis for Theorem 2.3; the technical details are left to interested readers.

Theorem 3.4. *For any time $T^*>0$, we assume that exact solution $\mathbf{u}_e$ to the harmonic mapping flow equation (1.2) satisfies the regularity requirement $\mathbf{u}_e\in H^4(0,T;H^3)\cap L^\infty(0,T;H^6)$. We denote the $\mathbf{u}_{\Delta t,h}$ as the continuous function as the extension of the fully discrete numerical solution obtained by (2.13). As $\Delta t, h\to 0$ under a linear refinement requirement $\Delta t\le Ch$, we obtain the following result:*

$$\|\mathbf{u}_{\Delta t,h}-\mathbf{u}_e\|_{\ell^\infty(0,T^*;\ell^2)}+\|\mathbf{u}_{\Delta t,h}-\mathbf{u}_e\|_{\ell^2(0,T^*;H_h^1)}\le C(\Delta t^4+h^4). \tag{3.34}$$

4. The numerical results

We present some numerical examples in this section, to demonstrate the stability and convergence of the proposed scheme. An exact profile is artificially constructed. Since the exact solution has the properties that if $|\mathbf{u}(\cdot,t)|\equiv 1$ at any time $t>0$, we construct a two-dimensional (2-D) exact profile as

$$\mathbf{u}_e=\begin{bmatrix}u\\ v\end{bmatrix}=\begin{bmatrix}\cos\Big(\cos(\pi x)\cos(\pi y)\cos t\Big)\\ \sin\Big(\cos(\pi x)\cos(\pi y)\cos t\Big)\end{bmatrix}, \tag{4.1}$$

with $\Omega=[0,1]\times[0,1]$. Notice that the homogeneous Neumann boundary condition is satisfied for the constructed profile.

As mentioned above, it is obvious that (4.1) is not an exact solution for the original harmonic mapping system (1.2), so that we have to add an artificial source modification term $\mathbf{f}$ to make the PDE exactly satisfied. In more detail, the PDE system (1.2) is modified as

$$\begin{bmatrix}u_t\\ v_t\end{bmatrix}-\begin{bmatrix}\Delta u\\ \Delta v\end{bmatrix}=\begin{bmatrix}(|\nabla u|^2+|\nabla v|^2)u\\ (|\nabla u|^2+|\nabla v|^2)v\end{bmatrix}+\begin{bmatrix}f_1\\ f_2\end{bmatrix}, \tag{4.2}$$

and a careful calculation reveals that

$$\mathbf{f}=\begin{bmatrix}f_1\\ f_2\end{bmatrix}=\begin{bmatrix}u_t-\Delta u-(|\nabla u|^2+|\nabla v|^2)u\\ v_t-\Delta v-(|\nabla u|^2+|\nabla v|^2)v\end{bmatrix}. \tag{4.3}$$

In the time evolution on both sides, a three-point Simpson's integration formula (over the time interval (t^n,t^{n+1})) will be used for $\mathbf{f}$ to minimize the numerical integration error.

4.1. Numerical error in space

To verify the accuracy in space, the time size Δt must be small enough to ensure that the numerical error is dominated by the spatial one. We will take the domain $[0,1]\times[0,1]$ and let $T=1$, with a fixed $\Delta t=10^{-3}$. A sequence of spatial resolution will be taken: $N=24:8:96$, in this experiment. The expected spatial numerical accuracy assumption $e=Ch^k$ indicates that $\ln|e|=\ln C-k\ln N$, so that we make a log–log plot to demonstrate the spatial convergence order. The fitted line displayed in Fig. 1 shows an approximate slope of -4, which in turn verifies a nice fourth order spatial convergence order, in both the discrete ℓ^2 and ℓ^∞ norms. We also notice that the numerical values of the discrete ℓ^2 and ℓ^∞ errors for the component u are almost identical, so that there is no clear difference (between the two errors) on the plot, while such a difference for the component v becomes more obvious.

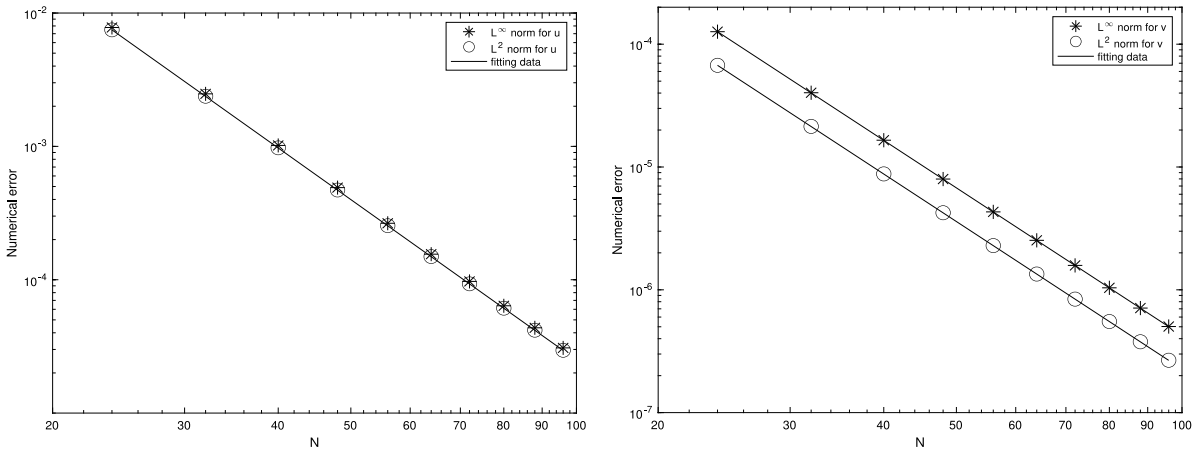

Fig. 1. The discrete ℓ^2 and ℓ^∞ numerical errors vs. spatial resolution N, for $N = 24 : 8 : 96$, with a fixed time step size $\Delta t = 10^{-3}$, for both components u and v.

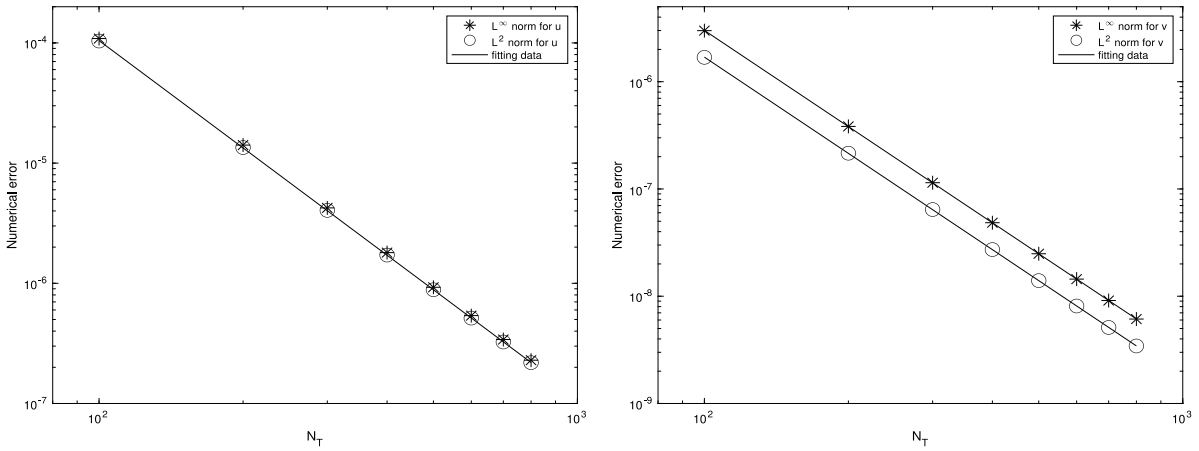

Fig. 2. The discrete ℓ^2 and ℓ^∞ numerical errors vs. temporal resolution $100N$, for $1 \le N \le 8$, with a fixed time step size $h = 10^{-3}$, for both components u and v.

4.2. Numerical error in time

To demonstrate the accuracy in time, the spatial numerical error has to be negligible. We fix the spatial resolution as $N = 1024$ (so that $h = \frac{1}{1024}$), and set the final time $T = 1$. Naturally, a sequence of time step sizes is taken as $\Delta t = \frac{T}{N_T}$, with $N_T = 100 : 100 : 800$. The expected temporal numerical accuracy assumption $e = C\Delta t^k$ indicates that $\ln|e| = \ln(CT^k) - k\ln N_T$, so that we plot $\ln|e|$ vs. $\ln N$ to demonstrate the temporal convergence order. The fitted line displayed in Fig. 2 shows an approximate slope of -3, which in turn verifies a nice third order temporal convergence order, in both the discrete ℓ^2 and ℓ^∞ norms. Again, it is observed that the numerical values of the discrete ℓ^2 and ℓ^∞ errors for the component u are almost identical, so that there is no clear difference (between the two errors) on the plot, while such a difference for the component v becomes more obvious.

4.3. Numerical accuracy check for the fourth order scheme

In the accuracy test for the fourth order scheme (2.13), we set the time size as $\Delta t = \frac{1}{2}h$, with $h = \frac{1}{N}$, so that the fourth order accuracy in both time and space could be confirmed. Again, the final time set as by $T = 1$. A sequence of spatial resolutions are taken as $N = 48 : 16 : 192$. The expected temporal numerical accuracy assumption $e = C(\Delta t^4 + h^4)$ indicates that $\ln|e| = \ln C - 24\ln N$, so that we plot $\ln|e|$ versus $\ln N$ to demonstrate the convergence order. The fitted line displayed in Fig. 3 shows an approximate slope of -4, which in turn verifies a perfect second convergence order, in both time and space.

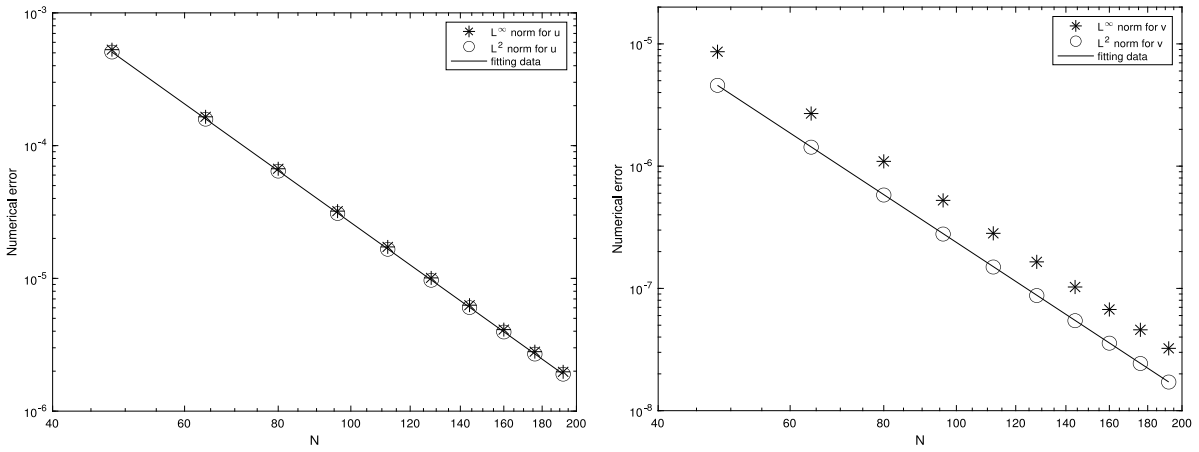

Fig. 3. The discrete ℓ^2 and ℓ^∞ numerical errors vs. spatial resolution N, for $N = 48 : 16 : 192$, with a time step size given by $\Delta t = \frac{1}{2}h$, for both components u and v, computed by the fourth order scheme (2.13).

5. Concluding remarks

In this article, a fully discrete numerical scheme is developed for the harmonic mapping flow (1.2), with the fourth order spatial accuracy and third order temporal accuracy. The fourth order spatial accuracy is realized via a long stencil finite difference, and a symmetric boundary extrapolation is applied, based on a higher order Taylor expansion around the boundary section. In the temporal discretization, a combination of explicit Adams–Bashforth extrapolation for the nonlinear terms and implicit Adams–Moulton interpolation for the viscous diffusion term is utilized, with third order accurate integration formula coefficients. This approach preserves the desired temporal accuracy order, while the numerical stability is assured by the subtle fact that, the diffusion coefficient at time step t^{n+1} dominates the rest coefficient sum. In addition, a detailed convergence analysis and error estimate are provided for the proposed numerical scheme, which gives an optimal $O(\Delta t^3 + h^4)$ accuracy order in the $\ell^\infty(0, T; \ell^2) \cap \ell^2(0, T; H_h^1)$ norm. A few numerical examples are also presented in this article, to demonstrate the full accuracy orders.

Acknowledgments

The authors greatly appreciate many helpful discussions with Hui Zhang, in particular for his insightful suggestions and comments. This work is supported in part by the grants NSF DMS-2012669 (C. Wang), NSFC-11771068, National Science Foundation of China-12071060 (L. Xu), National Science Foundation of China-11871139 (Z. Xia), National Science Foundation of China -11871105, 11571045 and Science Challenge Project, China TZ2018002 (Z. Zhang).

References

[1] J.L. Ericksen, Hydrostatic theory of liquid crystals, Arch. Ration. Mech. Anal. 9 (1962) 371–378.
[2] F.M. Leslie, Some constitutive equations for liquid crystals, Arch. Ration. Mech. Anal. 28 (1968) 265–283.
[3] M. Kružík, A. Prohl, Recent developments in modeling, analysis and numerics of ferromagnetism, SIAM Rev. 48 (2006) 439–483.
[4] F. Alouges, A new algorithm for computing liquid crystal stable configurations: the harmonic mapping case, SIAM J. Numer. Anal. 34 (1997) 1708–1726.
[5] S.Y. Lin, M. Luskin, Relaxation methods for liquid crystal problems, SIAM J. Numer. Anal. 26 (1989) 1310–1324.
[6] S. Bartels, A. Prohl, Constraint preserving implicit finite element discretization of harmonic map flow into spheres, Math. Comp. 76 (2007) 1847–1859.
[7] Y.M. Chen, The weak solutions to the evolution problems of harmonic maps, Math. Z. 201 (1989) 69–74.
[8] Y.M. Chen, M. Struwe, Existence and partial regularity results for the heat flow for harmonic maps, Math. Z. 201 (1999) 83–103.
[9] Y.M. Chen, W.Y. Ding, Blow-up and global existence for heat flows of harmonic maps, Invent. Math. 99 (1990) 567–578.
[10] Y.M. Chen, F.H. Lin, Evolution of harmonic maps with Dirichlet boundary conditions, Comm. Anal. Geom. 1 (1993).
[11] J.M. Coron, Nonuniqueness for the heat flow of harmonic maps, Ann. Inst. Henri Poincaré Anal. Non Linéaire 7 (1990) 335–344.
[12] M. Struwe, On the evolution of harmonic mappings of Riemannian surfaces, Comment. Math. Helv. 60 (1985) 558–581.
[13] J. Chen, C. Xie, C. Wang, Convergence analysis of a second-order semi-implicit projection method for Landau-Lifshiz equation, Appl. Numer. Math. 168 (2021) 55–74.
[14] C. Xie, C.J. Garciá-Cervera, C. Wang, Z. Zhou, J. Chen, Second-order semi-implicit projection methods for micromagnetics simulations, J. Comput. Phys. 404 (2020) 109104.
[15] S. Bartels, Stability and convergence of finite element approximation schemes for harmonic maps, SIAM J. Numer. Anal. 43 (2005) 220–238.
[16] A. Vese, J. Osher, Numerical methods for p-harmonic flows and approximations to image processing, SIAM J. Numer. Anal. 40 (6) (2002) 2085–2104.
[17] J.W. Barrett, S. Bartels, X. Feng, A. Prohl, A convergence and constant-preserving finite element method for the p-harmonic flow into spheres, SIAM J. Numer. Anal. 45 (3) (2007) 905–927.

[18] J.W. Barrett, X. Feng, A. Prohl, On p-harmonic heat flow for $1 \leq p < \infty$ and their finite element approximations, SIAM J. Math. Anal. 40 (4) (2008) 1471–1498.
[19] C. Luo, H. Zhang, Z. Zhang, Motion of singularities in the heat flow of harmonic maps into a sphere, East Asian J. Appl. Math. 9 (3) (2019) 580–600.
[20] J.-G. Liu, C. Wang, A fourth order numerical method for the primitive equations formulated in mean vorticity, Commun. Comput. Phys. 4 (2008) 26–66.
[21] J.-G. Liu, C. Wang, H. Johnston, A fourth order scheme for incompressible Boussinesq equations, J. Sci. Comput. 18 (2003) 253–285.
[22] R. Samelson, R. Temam, C. Wang, S. Wang, A fourth order numerical method for the planetary geostrophic equations with inviscid geostrophic balance, Numer. Math. 107 (2007) 669–705.
[23] C. Wang, J.-G. Liu, H. Johnston, Analysis of a fourth order finite difference method for incompressible Boussinesq equations, Numer. Math. 97 (2004) 555–594.
[24] K. Cheng, W. Feng, C. Wang, S.M. Wise, An energy stable fourth order finite difference scheme for the Cahn-Hilliard equation, J. Comput. Appl. Math. 362 (2019) 574–595.
[25] A. Fathy, C. Wang, J. Wilson, S. Yang, A fourth order difference scheme for the Maxwell equations on Yee grid, J. Hyperbolic Differ. Equ. 5 (2008) 613–642.
[26] S. Gottlieb, C. Wang, Stability and convergence analysis of fully discrete Fourier collocation spectral method for 3-D viscous Burgers' equation, J. Sci. Comput. 53 (2012) 102–128.
[27] K. Cheng, C. Wang, Long time stability of high order multi-step numerical schemes for two-dimensional incompressible Navier–Stokes equations, SIAM J. Numer. Anal. 54 (2016) 3123–3144.
[28] B. Fornberg, Generation of finite difference formulas on arbitrarily spaced grids, Math. Comp. 184 (1988) 699–706.
[29] B. Fornberg, Classroom note: Calculation of weights in finite difference formulas, SIAM Rev. 40 (1998) 685–691.
[30] A. Iserles, A First Course in the Numerical Analysis of Differential Equations, Cambridge University Press, Cambridge, 2009.
[31] S.A. Orszag, C.M. Bender, Advanced Mathematical Methods for Scientists and Engineers, Mac Graw Hill, 1978.
[32] J. Boyd, Chebyshev and Fourier Spectral Methods, Dover, New York, 2001.
[33] W. Chen, S. Conde, C. Wang, X. Wang, S.M. Wise, A linear energy stable scheme for a thin film model without slope selection, J. Sci. Comput. 52 (2012) 546–562.
[34] W. Chen, C. Wang, X. Wang, S.M. Wise, A linear iteration algorithm for energy stable second order scheme for a thin film model without slope selection, J. Sci. Comput. 59 (2014) 574–601.
[35] W. Chen, W. Li, Z. Luo, C. Wang, X. Wang, A stabilized second order ETD multistep method for thin film growth model without slope selection, Math. Model. Numer. Anal. 54 (2020) 727–750.
[36] K. Cheng, W. Feng, S. Gottlieb, C. Wang, A fourier pseudospectral method for the "Good" Boussinesq equation with second-order temporal accuracy, Numer. Methods Partial Differential Equations 31 (2015) 202–224.
[37] K. Cheng, Z. Qiao, C. Wang, A third order exponential time differencing numerical scheme for no-slope-selection epitaxial thin film model with energy stability, J. Sci. Comput. 81 (1) (2019) 154–185.
[38] K. Cheng, C. Wang, S.M. Wise, An energy stable Fourier pseudo-spectral numerical scheme for the square phase field crystal equation, Commun. Comput. Phys. 26 (2019) 1335–1364.
[39] K. Cheng, C. Wang, S.M. Wise, A weakly nonlinear energy stable scheme for the strongly anisotropic Cahn-Hilliard system and its convergence analysis, J. Comput. Phys. (2019) (in press).
[40] K. Cheng, C. Wang, S.M. Wise, X. Yue, A second-order, weakly energy-stable pseudo-spectral scheme for the Cahn-Hilliard equation and its solution by the homogeneous linear iteration method, J. Sci. Comput. 69 (2016) 1083–1114.
[41] C. Duan, C. Liu, C. Wang, X. Yue, Convergence analysis of a numerical scheme for the porous medium equation by an energetic variational approach, Numer. Math. Theory Methods Appl. 13 (2020) 63–80.
[42] Z. Guan, J. Lowengrub, C. Wang, Convergence analysis for second order accurate schemes for the periodic nonlocal Allen-Cahn and Cahn-Hilliard equations, Math. Methods Appl. Sci. 40 (2017) 6836–6863.
[43] Z. Guan, C. Wang, S.M. Wise, A convergent convex splitting scheme for the periodic nonlocal Cahn-Hilliard equation, Numer. Math. 128 (2014) 377–406.
[44] R. Samelson, R. Temam, C. Wang, S. Wang, Surface pressure Poisson equation formulation of the primitive equations: Numerical schemes, SIAM J. Numer. Anal. 41 (2003) 1163–1194.
[45] C. Wang, J.-G. Liu, Convergence of gauge method for incompressible flow, Math. Comp. 69 (2000) 1385–1407.
[46] L. Wang, W. Chen, C. Wang, An energy-conserving second order numerical scheme for nonlinear hyperbolic equation with an exponential nonlinear term, J. Comput. Appl. Math. 280 (2015) 347–366.